Dawn-Dusk Asymmetries in Planetary Plasma Environments

Stein Haaland, Andrei Runov, and Colin Forsyth
Editors

AGU American Geophysical Union

WILEY

Geophysical Monograph Series

180 **Arctic Sea Ice Decline: Observations, Projections, Mechanisms, and Implications** *Eric T. DeWeaver, Cecilia M. Bitz, and L.-Bruno Tremblay (Eds.)*
181 **Midlatitude Ionospheric Dynamics and Disturbances** *Paul M. Kintner, Jr., Anthea J. Coster, Tim Fuller-Rowell, Anthony J. Mannucci, Michael Mendillo, and Roderick Heelis (Eds.)*
182 **The Stromboli Volcano: An Integrated Study of the 2002–2003 Eruption** *Sonia Calvari, Salvatore Inguaggiato, Giuseppe Puglisi, Maurizio Ripepe, and Mauro Rosi (Eds.)*
183 **Carbon Sequestration and Its Role in the Global Carbon Cycle** *Brian J. McPherson and Eric T. Sundquist (Eds.)*
184 **Carbon Cycling in Northern Peatlands** *Andrew J. Baird, Lisa R. Belyea, Xavier Comas, A. S. Reeve, and Lee D. Slater (Eds.)*
185 **Indian Ocean Biogeochemical Processes and Ecological Variability** *Jerry D. Wiggert, Raleigh R. Hood, S. Wajih A. Naqvi, Kenneth H. Brink, and Sharon L. Smith (Eds.)*
186 **Amazonia and Global Change** *Michael Keller, Mercedes Bustamante, John Gash, and Pedro Silva Dias (Eds.)*
187 **Surface Ocean–Lower Atmosphere Processes** *Corinne Le Quèrè and Eric S. Saltzman (Eds.)*
188 **Diversity of Hydrothermal Systems on Slow Spreading Ocean Ridges** *Peter A. Rona, Colin W. Devey, Jérôme Dyment, and Bramley J. Murton (Eds.)*
189 **Climate Dynamics: Why Does Climate Vary?** *De-Zheng Sun and Frank Bryan (Eds.)*
190 **The Stratosphere: Dynamics, Transport, and Chemistry** *L. M. Polvani, A. H. Sobel, and D. W. Waugh (Eds.)*
191 **Rainfall: State of the Science** *Firat Y. Testik and Mekonnen Gebremichael (Eds.)*
192 **Antarctic Subglacial Aquatic Environments** *Martin J. Siegert, Mahlon C. Kennicut II, and Robert A. Bindschadler*
193 **Abrupt Climate Change: Mechanisms, Patterns, and Impacts** *Harunur Rashid, Leonid Polyak, and Ellen Mosley-Thompson (Eds.)*
194 **Stream Restoration in Dynamic Fluvial Systems: Scientific Approaches, Analyses, and Tools** *Andrew Simon, Sean J. Bennett, and Janine M. Castro (Eds.)*
195 **Monitoring and Modeling the Deepwater Horizon Oil Spill: A Record-Breaking Enterprise** *Yonggang Liu, Amy MacFadyen, Zhen-Gang Ji, and Robert H. Weisberg (Eds.)*
196 **Extreme Events and Natural Hazards: The Complexity Perspective** *A. Surjalal Sharma, Armin Bunde, Vijay P. Dimri, and Daniel N. Baker (Eds.)*
197 **Auroral Phenomenology and Magnetospheric Processes: Earth and Other Planets** *Andreas Keiling,* **Eric Donovan, Fran Bagenal, and Tomas Karlsson (Eds.)**
198 **Climates, Landscapes, and Civilizations** *Liviu Giosan, Dorian Q. Fuller, Kathleen Nicoll, Rowan K. Flad, and Peter D. Clift (Eds.)*
199 **Dynamics of the Earth's Radiation Belts and Inner Magnetosphere** *Danny Summers, Ian R. Mann, Daniel N. Baker, and Michael Schulz (Eds.)*
200 **Lagrangian Modeling of the Atmosphere** *John Lin (Ed.)*
201 **Modeling the Ionosphere-Thermosphere** *Jospeh D. Huba, Robert W. Schunk, and George V Khazanov (Eds.)*
202 **The Mediterranean Sea: Temporal Variability and Spatial Patterns** *Gian Luca Eusebi Borzelli, Miroslav Gacic, Piero Lionello, and Paola Malanotte-Rizzoli (Eds.)*
203 **Future Earth - Advancing Civic Understanding of the Anthropocene** *Diana Dalbotten, Gillian Roehrig, and Patrick Hamilton (Eds.)*
204 **The Galápagos: A Natural Laboratory for the Earth Sciences** *Karen S. Harpp, Eric Mittelstaedt, Noémi d'Ozouville, and David W. Graham (Eds.)*
205 **Modeling Atmospheric and Oceanic Flows: Insights from Laboratory Experiments and Numerical Simulations** *Thomas von Larcher and Paul D. Williams (Eds.)*
206 **Remote Sensing of the Terrestrial Water Cycle** *Venkat Lakshmi (Eds.)*
207 **Magnetotails in the Solar System** *Andreas Keiling, Caitríona Jackman, and Peter Delamere (Eds.)*
208 **Hawaiian Volcanoes: From Source to Surface** Rebecca *Carey, Valerie Cayol, Michael Poland, and Dominique Weis (Eds.)*
209 **Sea Ice: Physics, Mechanics, and Remote Sensing** *Mohammed Shokr and Nirmal Sinha (Eds.)*
210 **Fluid Dynamics in Complex Fractured-Porous Systems** *Boris Faybishenko, Sally M. Benson, and John E. Gale (Eds.)*
211 **Subduction Dynamics: From Mantle Flow to Mega Disasters** *Gabriele Morra, David A. Yuen, Scott King, Sang Mook Lee, and Seth Stein (Eds.)*
212 **The Early Earth: Accretion and Differentiation** *James Badro and Michael Walter (Eds.)*
213 **Global Vegetation Dynamics: Concepts and Applications in the MC1 Model** *Dominique Bachelet and David Turner (Eds.)*
214 **Extreme Events: Observations, Modeling and Economics** *Mario Chavez, Michael Ghil, and Jaime Urrutia-Fucugauchi (Eds.)*
215 **Auroral Dynamics and Space Weather** *Yongliang Zhang and Larry Paxton (Eds.)*
216 **Low-Frequency Waves in Space Plasmas** *Andreas Keiling, Dong-Hun Lee, and Valery Nakariakov (Eds.)*
217 **Deep Earth: Physics and Chemistry of the Lower Mantle and Core** *Hidenori Terasaki and Rebecca A. Fischer (Eds.)*
218 **Integrated Imaging of the Earth: Theory and Applications** *Max Moorkamp, Peter G. Lelievre, Niklas Linde, and Amir Khan (Eds.)*
219 **Plate Boundaries and Natural Hazards** *Joao Duarte and Wouter Schellart (Eds.)*
220 **Ionospheric Space Weather: Longitude and Hemispheric Dependences and Lower Atmosphere Forcing Timothy Fuller-Rowell,** *Endawoke Yizengaw, Patricia H. Doherty, and Sunanda Basu (Eds.)*
221 **Terrestrial Water Cycle and Climate Change Natural and Human-Induced Impacts** *Qiuhong Tang Taikan Oki*
222 **Magnetosphere-Ionosphere Coupling in the Solar System** *Charles R. Chappell, Robert W. Schunk, Peter M. Banks, James L. Burch, Richard M. Thorne (Eds.)*
223 **Natural Hazard Uncertainty Assessment: Modeling and Decision Support** *Karin Riley, Peter Webley, Matthew Thompson (Eds.)*
224 **Hydrodynamics of Time-Periodic Groundwater Flow: Diffusion Waves in Porous Media** *Joe S. Depner, Todd C. Rasmussen (Auth.)*
225 **Active Global Seismology** *Ibrahim Cemen and Yucel Yilmaz (Eds.)*
226 **Climate Extremes** *Simon Wang (Eds.)*
227 **Fault Zone Dynamic Processes** *Marion Thomas (Eds.)*
228 **Flood Damage Survey and Assessment: New Insights from Research and Practice** *Daniela Molinari, Scira Menoni, Francesco Ballio (Eds.)*
229 **Water-Energy-Food Nexus - Principles and Practices** *P. Abdul Salam, Sangam Shrestha, Vishnu Prasad Pandey, Anil K Anal*

Geophysical Monograph 230

Dawn-Dusk Asymmetries in Planetary Plasma Environments

Stein Haaland
Andrei Runov
Colin Forsyth
Editors

This Work is a co-publication of the American Geophysical Union and John Wiley and Sons, Inc.

AGU
American Geophysical Union

WILEY

This Work is a co-publication between the American Geophysical Union and John Wiley & Sons, Inc.

This edition first published 2017 by John Wiley & Sons, Inc., 111 River Street, Hoboken, NJ 07030, USA and the American Geophysical Union, 2000 Florida Avenue, N.W., Washington, D.C. 20009

Published under the aegis of the AGU Publications Committee
Brooks Hanson, Director of Publications
Robert van der Hilst, Chair, Publications Committee
For details about the American Geophysical Union visit us at www.agu.org.

Wiley Global Headquarters
111 River Street, Hoboken, NJ 07030, USA
For details of our global editorial offices, customer services, and more information about Wiley products visit us at www.wiley.com.

Library of Congress Cataloging-in-Publication data is available.

ISBN: 978-1-119-21632-2

Set in 10/12pt Times New Roman by SPi Global, Pondicherry, India

Printed in the United States of America.

10 9 8 7 6 5 4 3 2 1

CONTENTS

Part II: Internal Contributions to Dawn-Dusk Asymmetries

Part III: Dawn Dusk Asymmetries in Other Planets

CONTRIBUTORS

Brian J. Anderson
The Johns Hopkins University Applied Physics Laboratory, Laurel, Maryland, USA

Mats André
Swedish Institute of Space Physics, Uppsala, Sweden

Vassilis Angelopoulos
Department of Earth, Planetary, and Space Sciences, University of California, Los Angeles, California, USA

Sarah V. Badman
Department of Physics, Lancaster University, Bailrigg, Lancaster, United Kingdom

Jean Berchem
Department of Physics and Astronomy, University of California, Los Angeles, California, USA

Bertrand Bonfond
Laboratory for Planetary and Atmospheric Physics, STAR Institute, University of Liège, Liège, Belgium

Enrico Camporeale
Center for Mathematics and Computer Science (CWI) Amsterdam, Netherlands

James F. Carbary
The Johns Hopkins University Applied Physics Laboratory, Laurel, Maryland, USA

Emmanuel Chané
Centre for mathematical Plasma-Astrophysics, KU Leuven, Leuven, Belgium

Patrick W. Daly
Max Planck Institute for Solar System Research, Göttingen, Germany

Antoun G. Daou
Department of Physics and Astronomy, Rice University, Houston, Texas, USA

Johan De Keyser
Space Physics Division, Royal Belgian Institute for Space Aeronomy, Brussels, Belgium; *and* Center for mathematical Plasma-Astrophysics, Katholieke Universiteit Leuven, Leuven, Belgium

A. P. Dimmock
School of Electrical Engineering, Aalto University, Espoo, Finland

Eelco Doornbos
Delft Institute for Earth Observation and Space Systems (DEOS), Delft, Netherlands

Yusuke Ebihara
Research Institute for Sustainable Humanosphere, Kyoto University, Uji, Japan

C. Philippe Escoubet
European Space Agency, European Space Research and Technology Centre, Noordwijk, Netherlands

Matthias Förster
Helmholtz Centre Potsdam, GFZ German Research Centre for Geosciences, Potsdam, Germany

Christine Gabrielse
Department of Earth, Planetary, and Space Sciences, University of California, Los Angeles, California, USA

Elena E. Grigorenko
Space Research Institute, Russian Academy of Sciences, Moscow, Russia

Adrian Grocott
Department of Physics, Lancaster University, Bailrigg, Lancaster, UK

Denis Grodent
Laboratory for Planetary and Atmospheric Physics, STAR Institute, University of Liège, Liège, Belgium

Stein Haaland
Birkeland Center for Space Science, University of Bergen, Bergen, Norway; *and* Max Planck Institute for Solar System Research, Göttingen, Germany

Marc Hairston
Physics Department, University of Texas at Dallas, Richardson, Texas, USA

Doug Hamilton
University of Maryland, Department of Physics, College Park, Maryland, USA

Maria Hamrin
Department of Physics, Umeå University, Umeå, Sweden

Hiroshi Hasegawa
Department of Solar System Sciences, Institute of Space and Astronautical Science (ISAS), Japan Aerospace Exploration Agency (JAXA), Kanagawa, Japan

Ze-Jun Hu
SOA Key Laboratory for Polar Science, Polar Research Institute of China, Shanghai, China

Hong-Qiao Hu
SOA Key Laboratory for Polar Science, Polar Research Institute of China, Shanghai, China

Brian J. Jackel
Physics and Astronomy, University of Calgary, Calgary, Alberta, Canada

Jay R. Johnson
Andrews University, Berrien Springs, Michigan; *and* Plasma Physics Laboratory, Princeton University, Princeton, New Jersey, USA

Konstantin Kabin
Department of Physics, Royal Military College, University of Calgary, Calgary, Alberta, Canada

H. Karimabadi
University of California, San Diego, La Jolla, California; *and* SciberQuest, Inc. Del Mar, California, USA

Tomas Karlsson
Space and Plasma Physics, School of Electrical Engineering, KTH Royal Institute of Technology, Stockholm, Sweden

Amy M. Keesee
Department of Physics and Astronomy, West Virginia University, Morgantown, West Virginia, USA

S. Kiehas
Department of Earth, Planetary, and Space Sciences, University of California, Los Angeles, California, USA; *and* Space Research Institute, Austrian Academy of Sciences, Graz, Austria

Haje Korth
The Johns Hopkins University Applied Physics Laboratory, Laurel, Maryland, USA

Stamatios M. Krimigis
The Johns Hopkins University Applied Physics Laboratory, Laurel, Maryland, USA

Elena A. Kronberg
Max Planck Institute for Solar System Research, Göttingen, Germany; *and* Ludwig Maximilian University of Munich, Munich, Germany

Norbert Krupp
Max Planck Institute for Solar System Research, Göttingen, Germany

Anita Kullen
Space and Plasma Physics, School of Electrical Engineering, KTH Royal Institute of Technology, Stockholm, Sweden

Kun Li
Institute of Geology and Geophysics, Chinese Academy of Sciences, Beijing, China

S. S. Li
Department of Earth, Planetary, and Space Sciences, University of California, Los Angeles, California, USA; *and* Metromile, San Francisco, California, USA

William Longley
Rice Space Institute and Department of Physics and Astronomy, Rice University, Houston, Texas, USA; *and* Department of Astronomy, Boston University, MA, USA

Hao Luo
Key Laboratory of Ionospheric Environment, Institute of Geology and Geophysics, Chinese Academy of Sciences, Beijing, China

Larry R. Lyons
Department of Atmospheric and Oceanic Sciences, University of California, Los Angeles, California, USA

Lukas Maes
Space Physics Division, Royal Belgian Institute for Space Aeronomy, Brussels, Belgium

Romain Maggiolo
Space Physics Division, Royal Belgian Institute for Space Aeronomy, Brussels, Belgium

Göran Marklund
Space and Plasma Physics, School of Electrical Engineering, KTH Royal Institute of Technology Stockholm, Sweden

Kristofor M. Maynard
Space Science Center, University of New Hampshire, Durham, New Hampshire, USA

Donald G. Mitchell
The Johns Hopkins University Applied Physics Laboratory, Laurel, Maryland, USA

T. K. M. Nakamura
Space Research Institute, Austrian Academy of Sciences, Graz, Austria

Fritz M. Neubauer
Institut für Geophysik und Meteorologie, Universität zu Köln, Köln, Germany

Hans Nilsson
Swedish Institute of Space Physics, Kiruna, Sweden

K. Nykyri
Department of Physical Sciences, Embry-Riddle Aeronautical University, Daytona Beach, Florida, USA

A. Osmane
School of Electrical Engineering, Aalto University, Espoo, Finland

Benjamin Palmaerts
Max Planck Institute for Solar System Research, Göttingen, Germany; *and* Laboratory for Planetary and Atmospheric Physics, STAR Institute, University of Liege, Liege, Belgium

Timo Pitkänen
Department of Physics, Umeå University, Umeå, Sweden

Frederic Pitout
Institut de Recherche en Astrophysique et Planétologie, CNRS, Toulouse, France

Stefaan Poedts
Centre for mathematical Plasma-Astrophysics, KU Leuven, Leuven, Belgium

T. I. Pulkkinen
School of Electrical Engineering, Aalto University, Espoo, Finland

I. Jonathan Rae
Department of Space and Climate Physics, Mullard Space Science Laboratory, Holmbury St. Mary, Dorking, Surrey, United Kingdom

Joachim Raeder
Space Science Center, University of New Hampshire, Durham, New Hampshire, USA

Patricia Reiff
Rice Space Institute and Department of Physics and Astronomy, Rice University, Houston, Texas, USA

Robert L. Richard
Department of Physics and Astronomy, University of California, Los Angeles, California, USA

Andrei Runov
Department of Earth, Planetary, and Space Sciences, University of California, Los Angeles, California, USA

Abigail M. Rymer
The Johns Hopkins University Applied Physics Laboratory, Laurel, Maryland, USA

Joachim Saur
Institut für Geophysik und Meteorologie, Universität zu Köln, Köln, Germany

Mikhail I. Sitnov
The Johns Hopkins University Applied Physics Laboratory, Laurel, Maryland, USA

Emma Spanswick
Physics and Astronomy Department, University of Calgary, Calgary, Alberta, Canada

Grant K. Stephens
The Johns Hopkins University Applied Physics Laboratory, Laurel, Maryland, USA

Torbjörn Sundberg
School of Physics and Astronomy, Queen Mary University of London, London, United Kingdom

Nikolai A. Tsyganenko
Institute and Faculty of Physics, Saint-Petersburg State University, Saint-Petersburg, Russian Federation

Drew L. Turner
The Aerospace Corporation, El Segundo, California, USA

Aleksandr Y. Ukhorskiy
The Johns Hopkins University Applied Physics Laboratory, Laurel, Maryland, USA

Umberto Villante
Department of Physical and Chemical Sciences, University of L'Aquila, Italy

Marissa F. Vogt
Center for Space Physics, Boston University, Boston, Massachusetts, USA

Brian M. Walsh
Department of Mechanical Engineering and Center for Space Physics, Boston University, Boston, Massachusetts, USA

Chih-Ping Wang
Department of Atmospheric and Oceanic Sciences, University of California, Los Angeles, California, USA

Yong Wei
Institute of Geology and Geophysics, Chinese Academy of Sciences, Beijing, China

Simon Wing
The Johns Hopkins University Applied Physics Laboratory, Laurel, Maryland, USA

Xiaoyan Xing
XS Research LLC, Irvine, California, USA

Hui-Gen Yang
SOA Key Laboratory for Polar Science, Polar Research Institute of China, Shanghai, China

Bei-Chen Zhang
SOA Key Laboratory for Polar Science, Polar Research Institute of China, Shanghai, China

PREFACE

When a sphere is put into the path of a streaming fluid, one would expect an upstream stagnation point and a downstream wake region. One would also, at least to the first order, expect the diversion of the flow to be fairly rotationally symmetric about the flow direction. However, in the case of planetary bodies placed in the stream of solar-wind particles emanating from the Sun, there are a number of processes that can break this symmetry. Observations have shown that most planetary magnetospheres possess more or less pronounced dawn-dusk and north-south asymmetries in behavior and properties. Some of the asymmetries can be attributed to pure mechanics of the planets' celestial motion, the combined effects of a planet's orbital motion about the Sun and rotation around its own axis, but the added complication of the plasma-physical interaction between the planets and the solar wind mean that many cannot.

Some of the most intriguing sets of asymmetries arise due to properties of space itself. The universe is permeated by hot, highly turbulent magnetized plasma, while planetary bodies can have an intrinsic or induced magnetic field. These two factors give rise to another set of asymmetries, largely governed by electromagnetic forces, and far more unpredictable and dynamic than those caused by celestial mechanics.

The present volume is the outcome of a project initiated by a core group some years ago aiming to identify and quantify fundamental processes responsible for dawn-dusk asymmetries in planetary plasma environments. The work started out with a series of science sessions at the American Geophysical Union (AGU) fall meetings and an international team under the auspices of International Space Science Institute (ISSI) in Bern, Switzerland.

Both the contributors to the AGU sessions and the ISSI team members found the idea of compiling a volume dedicated to dawn-dusk asymmetries compelling, and agreed to contribute. Later during the process, additional specialists in the field were asked to contribute. The resulting volume contains 26 chapters authored and coauthored by more than 60 leading specialists and discusses observations, theories, and simulations of dawn-dusk asymmetries in planetary plasma environments.

In terms of organization, the volume starts out with asymmetries related to the interaction between the interplanetary space and the planetary magnetosphere, followed by asymmetries inside the magnetosphere. Most of our knowledge about dawn-dusk asymmetries stems from observations and simulations of the terrestrial magnetosphere. This is also reflected in many of the contributions, which focus on asymmetries in the terrestrial magnetosphere. However, many of the fundamental processes are universal, and apply to any planet. Three of the chapters are specifically dedicated to asymmetries in other planets. Although the book utilizes cross referencing, each chapter can be read as a stand-alone paper focusing on a specific aspect of dawn-dusk asymmetries.

This volume covers many of the key aspects of dawn-dusk asymmetries throughout the solar system, however there are still many unanswered questions. As our understanding of dawn-dusk asymmetries improves, we unlock new insights into the physical processes that drive and control planetary systems. As new missions, in particular to the outer planets, are realized and more sophisticated modeling possibilities evolve, new insight about our space environment, including asymmetries, can be expected. Color figures are available in the electronic version of this book.

Stein Haaland
Andrei Runov
Colin Forsyth

ACKNOWLEDGMENTS

The editors thank the authors for their contribution to this volume. More than 40 external reviewers took the time to carefully read through the chapters and provide valuable feedback to the authors.

We also thank the staff at John Wiley & Sons, Inc., in particular Dr. Ritu Bose and Mary Grace Hammond for their help during the editing and production of this volume.

Stein Haaland was supported by the Norwegian Research Council under grant BCSS 223252. Colin Forsyth was supported by the Natural Environment Research Council under grants NE/L007495/1, NE/M00886X/1, and NE/N014480/1. Andrei Runov was supported by NASA grants NNX13AF81G and NNX13AE10G, and NSF/GEM grant 1503097.

The editors also acknowledge support from the International Space Science Institute (ISSI), Bern, Switzerland.

ACRONYMS

AACGM	Altitude Adjusted Geomagnetic Coordinate System
ACE	Advanced Composition Explorer (satellite)
ADF	Antidipolarization Front in the Magnetotail
AE	Auroral Electrojet
AGSM	Aberrated Geocentric Solar Magnetic Coordinate System
AMPERE	Active Magnetosphere and Planetary Electrodynamics Response Experiment
AMPTE	Active Magnetospheric Particle Tracer Explorers and Ranging Mission
ARTEMIS	Acceleration, Reconnection, Turbulence, and Electrodynamics
ASI	All-Sky Imager
ATS	Applications Technology Satellite (satellite series)
AU	Astronomical Unit (1.5e8 km)
AWFC	Auroral Westward Flow Channel
BATS-R-US	Block-Adaptive-Tree-Solarwind-Roe-Upwind-Scheme (global MHD model)
BBELF	Broadband Extra Low Frequency Waves
BBF	Bursty Bulk Flow
CAPS	Cassini Plasma Spectrometer
CCMC	Community Coordinated Modeling Center
CEC	Corotation Enforcement Current System (Jupiter)
CEP	Cusp Energetic Particles
CHAMP	Challenging Minisatellite Payload
CHEMS	Charge-Energy-Mass Spectrometer (Cassini)
CIR	Coronal Interaction Region
CIS	Cluster Ion Spectrometry
CME	Coronal Mass Ejection
CODIF	Composition and Distribution Function Analyzer (Cluster)
CRCM	Comprehensive Ring Current Model
CRRES	Combined Release and Radiation Effects Satellite
DE-1, DE-2	Dynamics Explorer 1 and 2 (satellites)
DFB	Dipolarizing Flux Bundles in the Magnetotail
DMSP	Defense Meteorological Satellite Program
Dst	Disturbed Storm Time Index
DSX	Demonstration and Science Experiments (satellite series)
DTM	Drag Temperature Model
EDI	Electron Drift Instrument (Cluster and MMS)
EFW	Electric Field and Wave Instrument (Cluster)
EIC	Electrostatic Ion Cyclotron Waves
ELF	Extremely Low Frequency
ELS	Electron Spectrometer (Cassini)
EMIC	Electromagnetic Ion Cyclotron
ENA	Energetic Neutral Atom
EPD	Energetic Particle Detector (Galileo)
EPIC	Energetic Particles and Ion Composition (Geotail)
ERG	Energization and Radiation in Geospace (JAXA satellite)
ESA	Electrostatic Analyzer (THEMIS)
ESA	European Space Agency
EUV	Extreme Ultraviolet
FAC	Field Aligned Current
FAST	Fast Auroral Snapshot Explorer (NASA satellite)
FB	Foreshock Bubble (solar wind) and/or Flow Bursts (magnetotail)
FGM	FluxGate Magnetometer (Cluster)
FLR	Field Line Resonance and/or Finite Larmor Radius
FTE	Flux Transfer Event
FUV	Far Ultraviolet Spectrograph (Cassini)
GOCE	Gravity Field and Steady-State Ocean Circulation Explorer
GOES	Geostationary Operational Environmental Satellite (NOAA)
GRACE	Gravity Recovery and Climate Experiment
GSE	Geocentric Solar Ecliptic (coordinate system)
GSM	Geocentric Solar Magnetic (coordinate system)
GUVI	Global Ultraviolet Imager (TIMED satellite)
HEE	Hot Electron Enhancement
HFA	Hot Flow Anomaly
HIA	Hot Ion Analyzer (Cluster)
HSS	High-Speed Stream
HST	Hubble Space Telescope
ICME	Interplanetary Coronal Mass Ejection
IMAGE	Imager for Magnetopause-to-Aurora Global Exploration
IMF	Interplanetary Magnetic Field
IMP	Interplanetary Monitoring Platform (satellite series)
INCA	Ion-Neutral Camera (Cassini)
IR	Infrared

IRM	Ion Release Module (see AMPTE)
ISEE	International Sun-Earth Explorer (satellite series)
KH	Kelvin-Helmholtz
KHI	Kelvin-Helmholtz Instability
Kp	Magnetic Activity Index
LAD	Lyman Alpha Detector (TWINS satellite)
LAE	Low-Altitude Emissions
LANL	Los Alamos National Laboratory
LBH	Lyman-Birge-Hopfield
LEMMS	Low-Energy Magnetospheric Measurement System (Cassini)
LEP	Low-Energy Particle (GEOTAIL particle detector)
LFM	Lyon-Fedder-Mobarry (global MHD model)
LLBL	Low-Latitude Boundary Layer
LSK	Large-Scale Kinetic
LT	Local Time
MAG	Magnetic Field Instrument (Cassini)
MEPI	Medium Energy Particles Instrument
MESSENGER	Mercury Surface, Space Environment, Geochemistry, and Ranging Mission
MHD	Magnetohydrodynamic
MIMI	Magnetospheric Imaging Instrument (Cassini)
MLT	Magnetic Local Time
MMS	Magnetospheric Multiscale (satellite mission)
MSIS	Mass Spectrometer and Incoherent Scatter (model series)
MVABC	Constrained Minimum Variance Analysis
NASA	National Aeronautics and Space Administration
NCAR	National Center for Atmospheric Research
NENL	Near-Earth Neutral Line
NH	Northern Hemisphere
NOAA	National Oceanic and Atmospheric Administration
OGO	Orbiting Geophysical Observatories (NASA satellite series)
OpenGGCM	Open Geospace General Circulation Model
PAD	Pitch Angle Distribution
PBI	Poleward Boundary Intensifications
PBL	Plasmapause Boundary Layer
PCB	Polar Cap Boundary
PFN	Phase Front Normal
POES	Polar Operational Environmental Satellites
PSD	Power Spectral Density or Phase Space Density
PWOM	Polar Wind Outflow Model
RAPID	Research with Adaptive Particle Imaging Detector (Cluster)
RBSP	Radiation Belt Storm Probe (now Van Allen Probe)
RCM(-E)	Rice Convection Model (-Equilibrium)
RD	Rotational Discontinuity
RFT	Rapid Flux Transport in the Magnetotail
R_E	Earth Radii (6371 km)
R_J	Radius of Jupiter (69911 km)
R_M	Radius of Mercury (2440 km)
R_S	Radius of Saturn (60268 km)
SAID	Subauroral Ion Drift
SAPS	Subauroral Polarization Stream
SARAS	Substorm Associated Radar Auroral Surge
SCW	Substorm Current Wedge
SH	Southern Hemisphere
SI	Sudden Impulse
SMC	Steady Magnetospheric Convection
SST	Solid State Detector
SuperDARN	Super Dual Auroral Radar Network
SW	Solar Wind
TC-1	Double Star 1 (ESA/CNAS spacecraft)
TCR	Traveling Compression Region
TD	Tangential Discontinuity
THEMIS	Time History of Events and Macroscale Interactions During Substorms
TIGCM	Thermosphere Ionosphere General Circulation Model
TIMED	Thermosphere Ionosphere Mesosphere Energetics and Dynamics (satellite)
TRINNI	Tail Reconnection During IMF Northward, Nonsubstorm Intervals
TWINS	Two Wide-Angle Imaging Neutral Atom Spectrometers (satellite mission)
ULF	Ultralow Frequency
UT	Universal Time
UTC	Coordinated Universal Time (=UT)
UV	Ultraviolet
UVI	Ultraviolet Imager (Polar)
UVIS	Ultraviolet Imaging Spectrograph (Cassini)
VIS	Visible Imaging System (Polar)
WIC	Wideband Imaging Camera
WTS	Westward Traveling Surge

Part I
External Contributions to Dawn-Dusk Asymmetries

1

The Magnetosphere of the Earth under Sub-Alfvénic Solar Wind Conditions as Observed on 24 and 25 May 2002

Emmanuel Chané[1], Joachim Saur[2], Joachim Raeder[3], Fritz M. Neubauer[2], Kristofor M. Maynard[3], and Stefaan Poedts[1]

ABSTRACT

On 24 and 25 May 2002, the solar wind density was so low (<0.1 cm^{-3}), that the flow became sub-Alfvénic for intervals that lasted as long as 4 h (the Alfvén Mach number was as low as 0.4). The magnetosphere changed dramatically and (according to simulations and theory) became very asymmetric: the bow shock disappeared and two Alfvén wings formed on the flanks of the magnetosphere (the wings were 600 R_E long, the deceleration 30% in one wing and 60% in the other). Geotail's data suggest that it crossed one of these wings multiple times. The magnetosphere was geomagnetically extremely quiet, showed no substorm activity and almost no auroral activity. Simulations show that the closed field line region was very symmetric, extending to 20 R_E on the dayside and on the nightside. The open field lines became highly asymmetric: the field lines emanating from the Northern Hemisphere all pointed along the dawn Alfvén wing (around 8:00 LT), the field lines from the Southern Hemisphere all pointed along the other wing (around 22:00 LT). Between 28 November 1963 and 27 September 2015, there were 16 recorded sub-Alfvénic solar wind intervals, lasting for more than 1 h and caused by low solar wind density. Considering the uneven data coverage, these events occur, on average, every 2.2 years.

1.1. INTRODUCTION

Under typical solar wind conditions, the structure of Earth's magnetosphere can be characterized as follows: (1) compressed approximately dipolar magnetic field lines on the dayside that typically extend up to ~11 R_E, (2) elongated dipolar field lines on the nightside that form the magnetotail, and (3) the bow shock, located a few R_E upstream of the magnetopause, where the superfast (i.e., faster than the speed of the fast waves) solar wind plasma is abruptly decelerated, compressed, and heated. On very rare occasions (less than 20 times since 1969), the solar wind becomes sub-Alfvénic (i.e., slower than the speed of the Alfvén waves), and thus subfast, for a few hours. This is usually associated with periods where the density of the solar wind is very low. As a result, the configuration of the magnetosphere changes drastically: the bow shock disappears, the magnetopause standoff distance increases, and Alfvén wings form on both sides of the magnetosphere. Alfvén wings are tubular structures, that can be hundreds of R_E long, where the incoming plasma is slowed down, and where the magnetic field experiences a rotation [see *Drell et al*., 1965; *Neubauer*, 1980, 1998]. Alfvén wings are caused by standing Alfvén waves generated by an obstacle within a sub-Alfvénic plasma flow. The existence of Alfvén wings in the Earth environment was generally considered possible, but very

[1] *Centre for mathematical Plasma-Astrophysics, KU Leuven, Leuven, Belgium*

[2] *Institut für Geophysik und Meteorologie, Universität zu Köln, Köln, Germany*

[3] *Space Science Center, University of New Hampshire, Durham, New Hampshire, USA*

Dawn-Dusk Asymmetries in Planetary Plasma Environments, Geophysical Monograph 230, First Edition.
Edited by Stein Haaland, Andrei Runov, and Colin Forsyth.

unlikely, until *Chané et al*. [2012] presented the first observational evidence of Alfvén wings at Earth, which occurs during a sub-Alfvénic solar wind event in May 2002. A sketch of the Alfvén wings at Earth during that event is given in Figure 1.1. One wing is located on the dusk flank, whereas the other wing is on the dawn flank. Since the two wings are very different (e.g., orientation, plasma speed, magnetic field strength and orientation), they introduce a strong dawn-dusk asymmetry in the magnetosphere. The IMF almost always introduces an asymmetry in the magnetosphere, but the asymmetry is stronger when the solar wind Alfvén Mach number is low, and even stronger when the solar wind is sub-Alfvénic. Asymmetries in the magnetosphere during low-Alfvén-Mach-number solar wind intervals have been studied by *Lavraud et al*. [2007, 2013], *Lavraud and Borovsky* [2008], and *Nishino et al*. [2008] (although these studies did not consider the sub-Alfvénic case). *Nishino et al*. [2008] showed that drastic dawn-dusk asymmetries arose in the magnetosheath (also in the tail). *Lavraud et al*. [2007] showed that the magnetopause was asymmetric during low-Alfvén-Mach-number solar wind periods. They also showed that strong plasma acceleration could be present in the magnetosheath during these periods and that these accelerations were also not symmetric. *Lavraud and Borovsky* [2008] showed that low-Alfvén-Mach-number solar wind intervals generated asymmetric magnetosheath flows, as well as asymmetric shapes for the magnetopause and for the magnetotail. We will see in the present chapter how the dawn-dusk asymmetries are even more pronounced and how the configuration of the magnetosphere changes drastically once the solar wind becomes sub-Alfvénic.

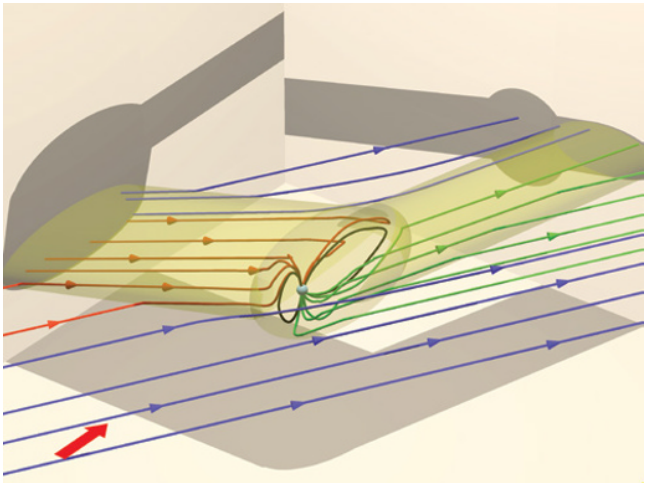

Figure 1.1 Three dimensional sketch of the Alfvén wings on 24 and 25 May 2002 showing: magnetic field lines (lines with arrows), the two Alfvén wings and the closed field line region (semitransparent areas). These regions are projected on three planes ($X = -210$ R_E, $Y = -180$ R_E, and $Z = -95$ R_E in GSE) to show the geometry of the wings. The direction of the incoming solar wind is shown by the flat arrow.

Although Alfvén wings are extremely uncommon at Earth, they may be less rare at Mercury, since the Alfvén and fast Mach number in the solar wind are usually lower at the orbit of Mercury [see *Sarantos and Slavin*, 2009]. Alfvén wings are also expected to be present at numerous exoplanets [see *Shkolnik et al*., 2003; *Saur et al*., 2013] and can even magnetically connect the planet and its parent star (which then produces an auroral footprint on the star, see *Preusse et al*., 2007; *Kopp et al*., 2011). Alfvén wings are also found in the solar system, at moons possessing an ionosphere and which are embedded in the magnetosphere of their parent planet (e.g., Io, Europa, Ganymede, Callisto, and Titan; see *Kivelson et al*., 2004). The Alfvén wings of these moons are known very well thanks to in situ measurements (obtained by the *Galileo* spacecraft at Jupiter, and by the *Cassini* spacecraft at Saturn), to theoretical studies, as well as numerical simulations. For objects without intrinsic dynamo fields such as Io and Europa, see *Linker et al*. [1988], *Saur et al*. [1999], *Frank and Paterson* [2000], *Schilling et al*. [2008], for objects with dynamo fields, that is, Ganymede see *Jia et al*. [2009] and *Duling et al*. [2014]. The Alfvén wings of these moons can generate a localized auroral spot (called footprint) in the ionosphere of their parent planet. These auroral footprints have been observed by the Hubble Space Telescope for Io, Europa, and Ganymede [*Clarke et al*., 2002; *Gérard et al*., 2002, 2006; *Bonfond et al*., 2007, 2008] as well as for Enceladus [*Pryor et al*., 2011].

In the present chapter, we will show how the Earth's magnetosphere changes when the solar wind is sub-Alfvénic and when Alfvén wings are present. In section 1.2, the concept of Alfvén wings is introduced in more detail: how are they generated? How do they affect the incoming plasma? How fast do they expand? In section 1.3, the prevalence of sub-Alfvénic conditions in the solar wind just upstream of the Earth is studied. Observational evidence of the presence of Alfvén wings at Earth on 24 and 25 May 2002 is presented in section 1.4. This event is then studied via MHD numerical simulations in section 1.5. Our concluding remarks are then presented in section 1.6.

1.2. ALFVÉN WINGS: THEORY

When an obstacle (e.g., the Earth, Io, Enceladus) is embedded in a plasma flow (e.g., the solar wind, Jupiter's or Saturn's plasma sheet), plasma waves are generated by

the momentum exchange between the obstacle and the plasma (e.g., fast, slow, and Alfvén waves). The fast waves propagate in all directions, although slightly faster when propagating perpendicularly to the magnetic field. In case of a superfast incoming flow, the fast waves are responsible for the formation of the bow shock.

On the other hand, the group velocity of the Alfvén waves is directed purely along the magnetic field lines (in both directions); this velocity is $\mathbf{v_A} = \mathbf{B}/\left(\mu_0\rho\right)^{\frac{1}{2}}$ in the rest frame of the unperturbed plasma. Here **B** is the magnetic field, ρ is the plasma mass density, and μ_0 is the vacuum permeability. These waves are also advected by the plasma flow at a velocity **v**, in the rest frame of the obstacle the Alfvén waves propagate in the directions $\mathbf{C_A^{\pm}} = \mathbf{v} \pm \mathbf{v_A}$, which are called the Alfvén characteristics. The Alfvén waves thus form a stationary wave field along the Alfvén characteristics called the Alfvén wings.

The wings can be affected by other waves (e.g., fast or slow waves) generated, for instance, by the bow shock or by the ionosphere. Pure Alfvén wings are therefore only present in regions where the fast waves and the slow waves can be neglected. This is not the case close to the bow shock, which is why pure Alfvén wings are only present when the incoming flow is subfast. This is also not the case close to the ionosphere (which also generates slow waves and fast waves). The region where the Alfvén waves are affected neither by the slow waves (because they propagate in a different region of space), nor by the fast waves (because sufficiently far from the region where fast waves are generated, their amplitude is very low) is called the far field region. Note that in the case of a sub-Alfvénic flow with a high plasma β, the slow waves and the Alfvén waves would propagate in the same direction and there would be no far field region. This situation is extremely unlikely to happen in the solar wind at the orbit of the Earth, but it might arise if the sub-Alfvénic flow would be caused by a very low plasma speed, for instance. We here consider ideal Alvén wings in a homogeneous and time-stationary plasma flow.

Because the Alfvén waves only propagate in one direction, their amplitude does not decrease during propagation (in contrast to fast waves), Alfvén wings are therefore translation invariant and can be very long structures. The wings propagate with the velocity $\mathbf{C_A^{\pm}}$, which is typically hundreds of km/s in the solar wind, and can thus, even for short periods of sub-Alfvénic incoming flow, acquire a considerable length.

As an example, let us consider an incoming plasma flow with a speed of 400 km/s and an Alfvén speed of 690 km/s, and where the magnetic field is perpendicular to the direction of propagation of the incoming flow. The Alfvén Mach number is then ~0.58. In this case, the angle between the wings and the direction of propagation of the incoming flow is the same for both wings. (Note that this is the symmetric case, since **v** and **B** are perpendicular in the solar wind. This is thus very different from the May 2002 event.) It is given by $\arctan(v_A/v) \approx 60°$. In this example, after 1 h of sub-Alfvénic incoming flow, the Alfvén wings would already be 450 R_E long.

Depending on the ionospheric conductivity of the obstacle, the Alfvén wings can affect the incoming flow strongly (high ionospheric conductance) or only weakly (low ionospheric conductance). For instance, in the hypothetical case of an infinite ionospheric Pedersen conductance, the plasma flow perpendicular to the magnetic field would come to a halt inside the Alfvén wings, and the magnetic field **B** and the plasma velocity **v** would be perfectly aligned with the wings axis C_A^+ and C_A^-. Knowing the upstream conditions and the ionospheric conductance, the analytical model of *Neubauer* [1980, 1998] can be used to derive the plasma velocity and the magnetic field inside the Alfvén wings. To do so, one can use equations (14), (15), and (26) from *Neubauer* [1980] and equation (A10) from *Saur et al*. [1999], neglecting the topological effects of the internal magnetic field of the Earth as a first approximation. Inside the wings, the plasma flow, for instance, is decreased by a factor $\alpha = 2\Sigma_A/\left(\Sigma_P + 2\Sigma_A\right)$, where Σ_P and Σ_A are the Pedersen conductance in the ionosphere and the Alfvén conductance in the solar wind, respectively. The Alfvén conductance is given by $1/\left(\mu_0 v_A\sqrt{1+M_A^2+2M_A\cos\theta}\right)$, where θ is the angle between **B** and **v** in the solar wind. In the previous example, the Alfvén conductance would then be 1 S, meaning that, for an ionospheric conductivity of 5 S, the flow would be 71% slower in the Alfvén wings than in the solar wind. In this simple symmetric example, the deceleration is the same in the dawn and in the dusk wing, this is not what usually happens, and not what happened during the May 2002 event. The electromagnetic energy (i.e., the Poynting vector) radiated away from the dawn and from the dusk wings is generally very different depending on the orientation of the IMF (see Fig. 5 in *Saur et al*., 2013).

Note that an obstacle without an ionosphere would also create Alfvén wings for a sub-Alfvénic incoming flow. The key property is that the obstacle perturbs the plasma flow perpendicular to the magnetic field.

1.3. PREVALENCE OF SUB-ALFVÉNIC SOLAR WIND CONDITIONS AT EARTH

For Alfvén wings to develop at Earth, the incoming solar wind Alfvén Mach number needs to be less than one. The Alfvén wings propagate with the Alfvén speed, and the longer the solar wind remains sub-Alfvénic, the longer the wings will be. A sub-Alfvénic event lasting 1 h, for instance, would generate wings hundreds of R_E long,

but such events are extremely rare. They are usually associated with periods of exceptionally low solar wind plasma density. *Usmanov et al*. [2005] studied the occurrence of low-density events upstream of the Earth. After analyzing four decades of hourly average data (between 1963 and 2003), they found 23 events where the solar wind density was lower than 0.3 cm^{-3}. Some of these intervals are only 1 h long, while others last for tens of hours. The longest low-density interval found lasted for 42 h. For nine of these time intervals, sub-Alfvénic flows were measured. But one should keep in mind that the data coverage during this time period was only 58% on average (as high as 100% in 2002, but as low as 7% in 1964). Extending the dataset of *Usmanov et al*. [2005] up to 20 August 2015, we found 16 sub-Alfvénic events caused by low solar wind density lasting for at least 1 h. So it seems that, on average, this kind of event occurs every 2.2 years (taking into account data coverage). But these events are not evenly distributed. For instance, three sub-Alfvénic events happened in 1979, and three others in 2002, while none were measured between 1980 and 1999 (but the data coverage was low between 1983 and 1994, since it was after ISEE-3, but before WIND).

In this section, we study in detail the seven most sub-Alfvénic of these events (i.e., the ones that reached the lowest M_A). The number density and the Alfvén Mach number measured during these events are shown in Figure 1.2. The two most spectacular events happened on 4 and 31 July 1979. These two events are probably linked since there is almost exactly one Carrington rotation (27.3 days) between them. On 4 July 1979, the solar wind was sub-Alfvénic for almost 10 consecutive hours, with values as low as 0.25 for M_A. During that time, the Alfvén wings would have reached the enormous length of 4000 R_E (0.17 AU). The solar wind density was extremely low during this event, most of the time below 0.1 cm^{-3} and sometimes as low as 0.025 cm^{-3}. It should be noted that for this event, the dawn and dusk wings must have been very different, introducing a strong dawn-dusk asymmetry in the magnetosphere. Figure 1.3 shows the measured angles between the interplanetary magnetic field and the Sun-Earth line in the ecliptic plane for the seven events studied here. One can see in this figure that the IMF was more or less along the Parker spiral during this event, meaning that the orientations of the Alfvén wings must have been more or less the same as the one displayed in Figure 1.1.

The second event, on 31 July 1979, lasted even longer: the solar wind was sub-Alfvénic for 15 consecutive hours (with M_A as low as 0.3). It was also caused by a low density solar wind, with values as low as 0.03 cm^{-3}. Again, due to the orientation of the IMF, the wings introduced a dawn-dusk asymmetry during this event (see Fig. 1.3).

The third sub-Alfvénic event in 1979 happened on 22 November. During this event, the solar wind was sub-Alfvénic for several intervals that lasted as long as 50 min. In total, M_A was below one for about 5 h. M_A was as low as 0.35, and n as low as 0.03 cm^{-3}. This event has been studied by *Gosling et al*. [1982]. Using data from ISEE-3 and ISEE-2, they concluded that the bow shock never disappeared during this event. Their conclusion is based on temperature and magnetic field strength measurements: higher values at ISEE-2 seems to indicate that the bow shock was present between the two spacecraft; however, each time that the solar wind displayed a low density and a low Alfvén Mach number, the magnetosphere expanded and ISEE-2 crossed the magnetopause, making any statement about the presence or the absence of the bow shock questionable.

The low-density event, which received the broadest attention with respect to publications, is without a doubt the day the solar wind almost disappeared [see *Le et al*., 2000a, 2000b; *Ohtani et al*., 2000; *Jordanova et al*., 2001; *Smith et al*., 2001; *Balasubramanian et al*., 2003], which happened on 11 May 1999. But somehow surprisingly, this event is not the most spectacular: the solar wind density is not as low as for the other events, neither is the solar wind Alfvén Mach number, and the event is not particularly long. The solar wind was sub-Alfvénic for several time periods, but none of them lasted for more than half an hour. M_A was as low as 0.7, and n as low as 0.07 cm^{-3}. The IMF was very close to the Parker spiral configuration: the angle between the IMF and the Sun-Earth line was between 40° and 45° for almost 70% of the measurements when the solar wind was sub-Alfvénic. As a result, the orientation of the wings must have been similar to Figure 1.1, with a strong dawn-dusk asymmetry.

There were three sub-Alfvénic events in 2002 that may or may not have been linked (there were approximately two Carrington rotations between the events). The one with the lowest density and with the lowest Alfvén Mach number occurred on 24 and 25 May 2002. This event is particularly interesting for several reasons. First of all, four spacecraft located in the solar wind on this day provide consistent and independent measurements of the low density (see Fig. 1.4). Having multiple observations available is important to rule out measurement errors because plasma density measurements may not be very accurate, especially when the particle flux is low [*Gosling et al*., 1982]. Having consistent measurements by four independent spacecraft provides high confidence that the solar wind really was sub-Alfvénic during this event. In addition, during this event, Geotail, which was orbiting the Earth, crossed the Alfvén wings several times, thus providing the first direct observational evidence of Alfvén wings at Earth. The next section is devoted entirely to this event. As can be seen in Figure 1.3, the orientation of the IMF was very different for these three events: close to 45° for the event in May, close to 120° for the event in March (meaning that Fig. 1.1 needs to be mirrored for this

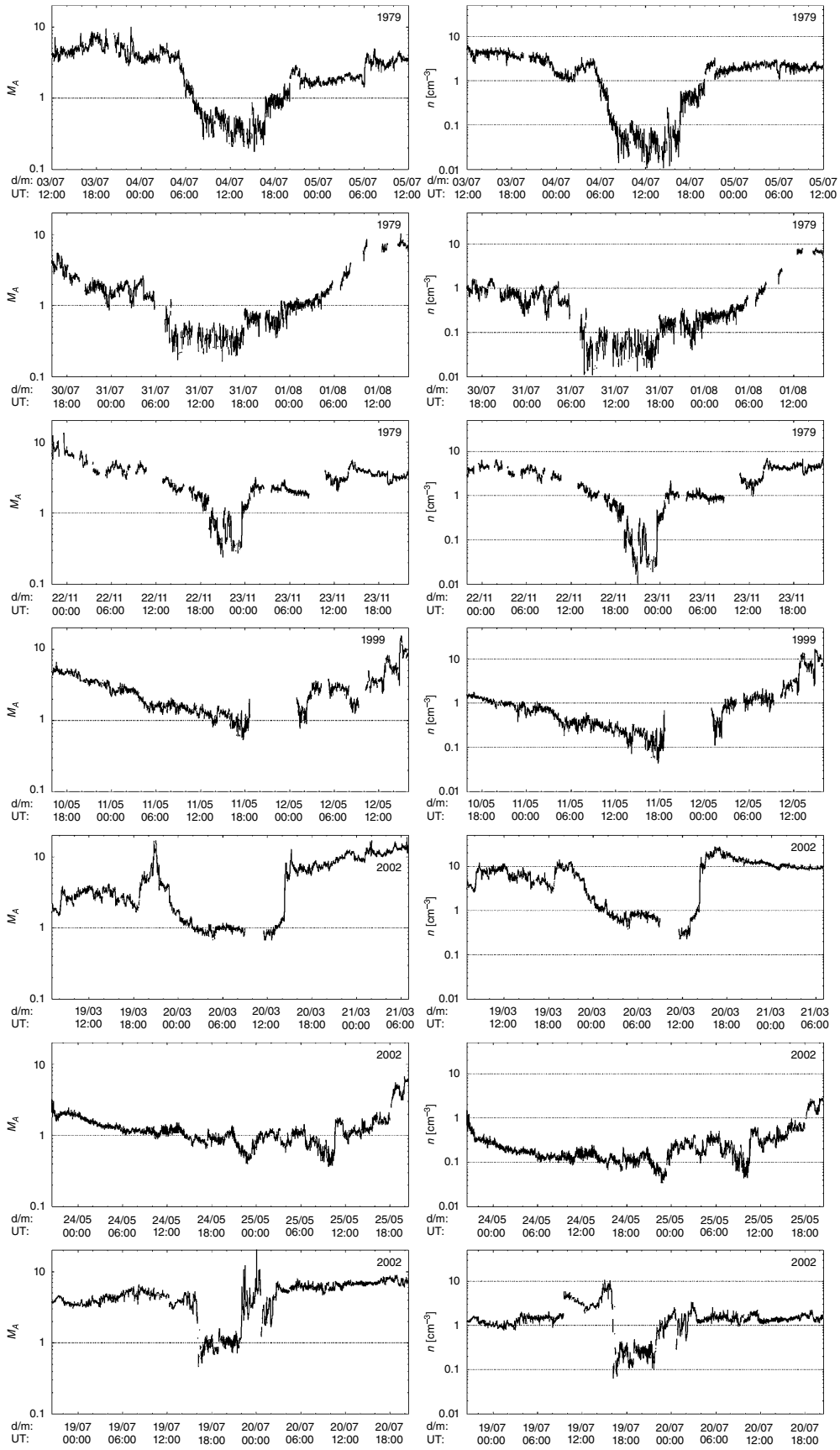

Figure 1.2 Alfvén Mach number (left panel) and number density (right panel) in the solar wind at L1 for seven events where the solar wind was sub-Alfvénic.

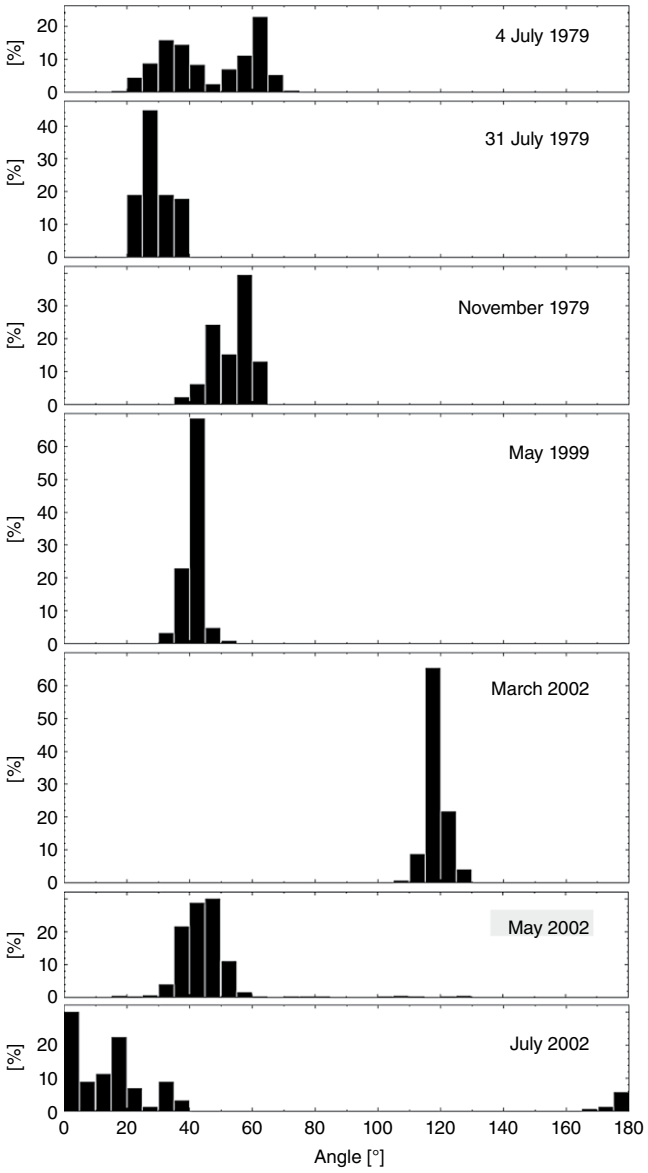

Figure 1.3 Histogram representing the different orientations of the IMF during sub-Alfvénic intervals for the seven events studied in the present chapter. An angle of 45° means the IMF is in a Parker spiral configuration (above or below the current sheet), an angle of 135° means that the IMF is perpendicular to the Parker spiral, angles of 0° or 180° means that the IMF is aligned with the Sun-Earth line. For instance, the histogram shows that during the March 2002 event, when the solar wind was sub-Alfvénic, 65% of the time, this angle was between 115° and 120°.

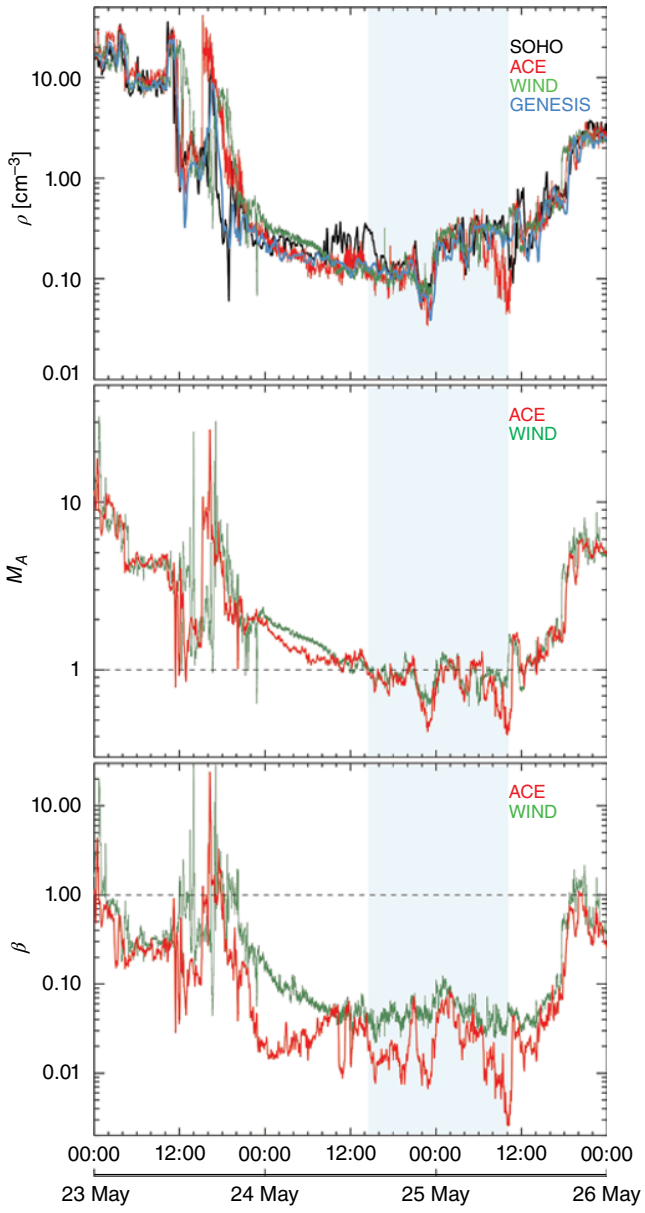

Figure 1.4 In situ measurements from several different spacecraft (SOHO, ACE, WIND, and GENESIS) in the solar wind on 24 and 25 May 2002. Top panel: number density; middle panel: Alfvén Mach number; bottom panel: plasma β. The dark background color highlights the period of very low density and very low Alfvén Mach number (mainly less than one).

event), close to 10° in July 2002. This also means that the event in July 2002 is the only one that does not introduce a dawn-dusk asymmetry in the magnetosphere (or only a slight asymmetry in comparison to the other events). Instead, the wings would display a strong day-night asymmetry, with one wing pointing toward the tail, and the second one more or less in the direction of the Sun.

1.4. ALFVÉN WINGS AT EARTH: OBSERVATIONAL EVIDENCE

The observational aspects of the May 2002 event were studied by *Chané et al.* [2012]. The solar wind density during this event was below 0.5 cm^{-3} for at least 40 h and sometimes as low as 0.04 cm^{-3} (see panel 1 of Fig. 1.4). Due to this very low density, the Alfvén Mach number became extremely low. M_A was lower than 1 for several

intervals lasting up to 4 h, and reached a minimum value of 0.4 (see panel 2 of Fig. 1.4). During this event, the solar wind speed and magnetic field were not unusual: plasma speeds between 300 and 850 km/s were measured, and the IMF strength was about 10 nT (with only low amplitude fluctuations). During this event, the plasma β was low, always between 0.003 and 0.1 (see panel 3 of Fig. 1.4). Such low values for β imply that the fast Mach number and the Alfvén Mach number were almost equal.

Due to the low solar wind ram pressure, the magnetopause expanded. Using the empirical model of *Shue et al*. [1998], one finds magnetopause standoff distances as high as 22 R_E. The position of the magnetopause can also be estimated by assuming a simple pressure balance between, on the one hand, the magnetic pressure of the Earth's dipole and, on the other hand, the ram pressure plus the magnetic pressure of the solar wind: values as high as 18 R_E are then found [see *Chané et al*., 2012].

Based on solar wind measurements on 24 May 2002 at 23:30 UT, *Chané et al*. [2012] calculated that the directions of the Alfvén wings in GSE coordinates were 0.13, −0.94, 0.32 for the dawn Alfvén wing and −0.82, 0.57, 0.03 for the dusk/tail Alfvén wing. The geometry of the wings is illustrated with a sketch in Figure 1.1, where one can see (1) that the wings are mostly in the equatorial plane, (2) that the field lines rotate when they enter or exit the wings, and (3) that all the field lines from the dawn Alfvén wing connect to the northern ionosphere, while all the field lines from the dusk/tail wing connect to the southern ionosphere. *Chané et al*. [2012] have also calculated that, according to theory [see *Neubauer*, 1980, 1998; *Saur et al*., 1999], the plasma speed in the dawn and in the dusk wing was 43% and 70% of the solar wind speed, respectively. One can see that there is a strong difference in the orientation of the wings and that the wings characteristics (e.g., flow speed, magnetic field strength and orientation) are also very different in the two wings. This means that the dawn-dusk asymmetries were very pronounced. *Chané et al*. [2015] also estimated that the wings reached a size of 600 R_E.

Chané et al. [2012] used Geotail's measurements to confirm that the bow shock disappeared and that Alfvén wings were present. Geotail was located on the dusk side, at about 30 R_E during this event. The magnetic field strength measured by Geotail was lower than the one measured in the solar wind, thus confirming that the bow shock was not present. The Alfvén wings crossed Geotail 36 times: the measurements show that the magnetic field rotates, and that the plasma decelerates inside the wing, as predicted by theory. The minimum variance analysis [see *Sonnerup and Cahill*, 1967] could be applied for nine crossings (the eigenvalue ratio was not large enough for the other cases) and it was found that the normals to these discontinuities were all perpendicular to the theoretical axis of the wings (thus confirming that Alfvén wing crossings were observed). *Chané et al*. [2012] also analyzed IMAGE WIC images and found essentially no auroral activity during this event. Measurements from DMSP F13 passes over the polar caps were also inspected, revealing that electron and proton precipitation fluxes were much lower than normal. The magnetosphere was thus geomagnetically extremely quiet during this event.

1.5. NUMERICAL SIMULATIONS

Recently, *Chané et al*. [2015] performed global 3D MHD simulations of the May 2002 event. They studied how the transition from a super-Alfvénic to a sub-Alfvénic solar wind affects the bow shock, the magnetopause, and the magnetotail; how the ionospheric currents changed; and how the open and the closed magnetic field lines are affected by this transition. OpenGGCM, a code that solves the ideal MHD equations in semiconservative form and where the ionosphere is treated as an infinitely thin layer below the inner boundary [see *Raeder et al*., 1995, 2006, 2008; *Raeder*, 2003], was used to perform the simulations

Figure 1.5 shows the result of a simulation where an incoming solar wind with the following properties was considered: a density of 0.04 cm^{-3}, a plasma speed of 480 km/s, and a magnetic field given by $\mathbf{B}$ =(−7.2,7.3,1.0) nT in GSE coordinates; this corresponds to an Alfvén Mach number of 0.4. These values were measured in the solar wind by ACE on 24 May at 23:00 UT. In this figure, the two Alfvén wings can clearly be seen and display a drop in plasma speed, as well as an increase in B_x in the dawn wing, and a drop of B_x in the dusk wing (as expected by theory, see *Neubauer*, 1980, 1998). The figure also shows that all the open field lines of the dawn Alfvén wing are connected to the Northern Hemisphere, and that those of the dusk Alfvén wing are connected to the Southern Hemisphere.

Figure 1.6 shows how the magnetic field configuration drastically changed when the solar wind became sub-Alfvénic. One can see, for instance, how the closed field lines evolved from a typical super-Alfvénic ($M_A = 4.8$) situation (elongated in the tail and compressed on the dayside) to a sub-Alfvénic situation: the size of the magnetotail has shrunk and the field lines only extend up to about 20 R_E instead of almost 100 R_E at the beginning of the simulation, while conversely on the dayside the field lines have expanded from ~13 to ~20 R_E. As a result, the closed field line region became very symmetric. This is easy to understand, since M_A^2 is proportional to the ratio between the ram pressure and the magnetic pressure. When the solar wind Alfvén Mach number is large, the solar wind ram pressure is much stronger than the solar wind magnetic pressure. In this case, the magnetosphere

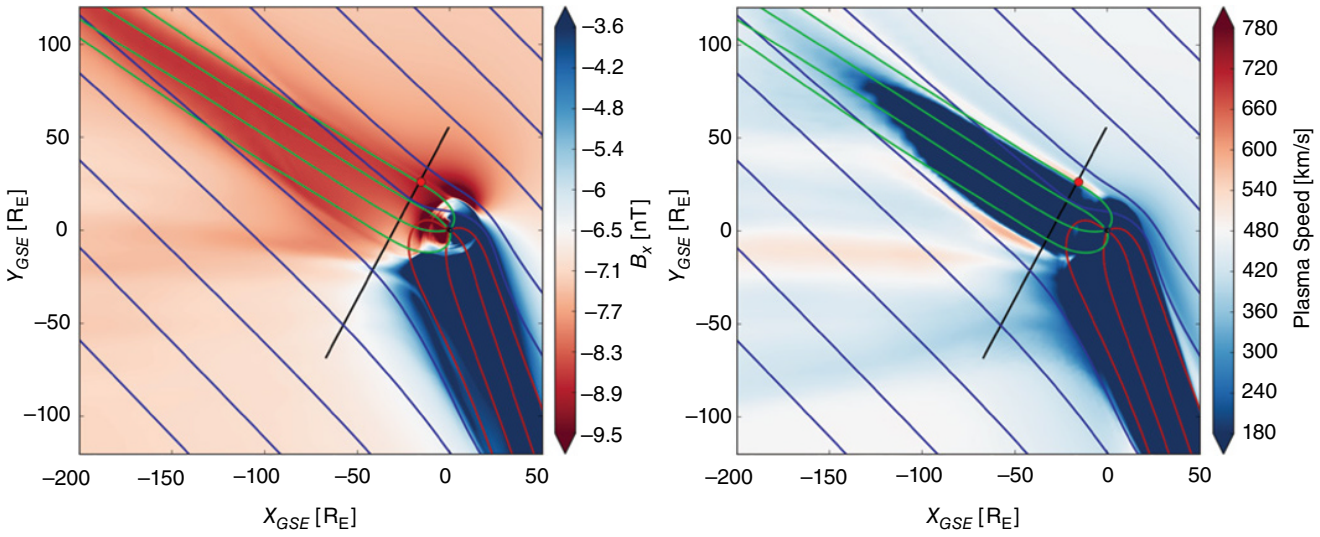

Figure 1.5 Top view of the field lines and color coded B_x (left panel) and color coded plasma speed (right panel) in the equatorial plane for the simulation performed by *Chané et al.* [2015]. The solar wind is coming from the right. The dot represents the position of Geotail on 24 May 2002 at 23:00 UTC. The dark line passing through this dot shows a plane across the dusk Alfvén wing that intersects Geotail's position.

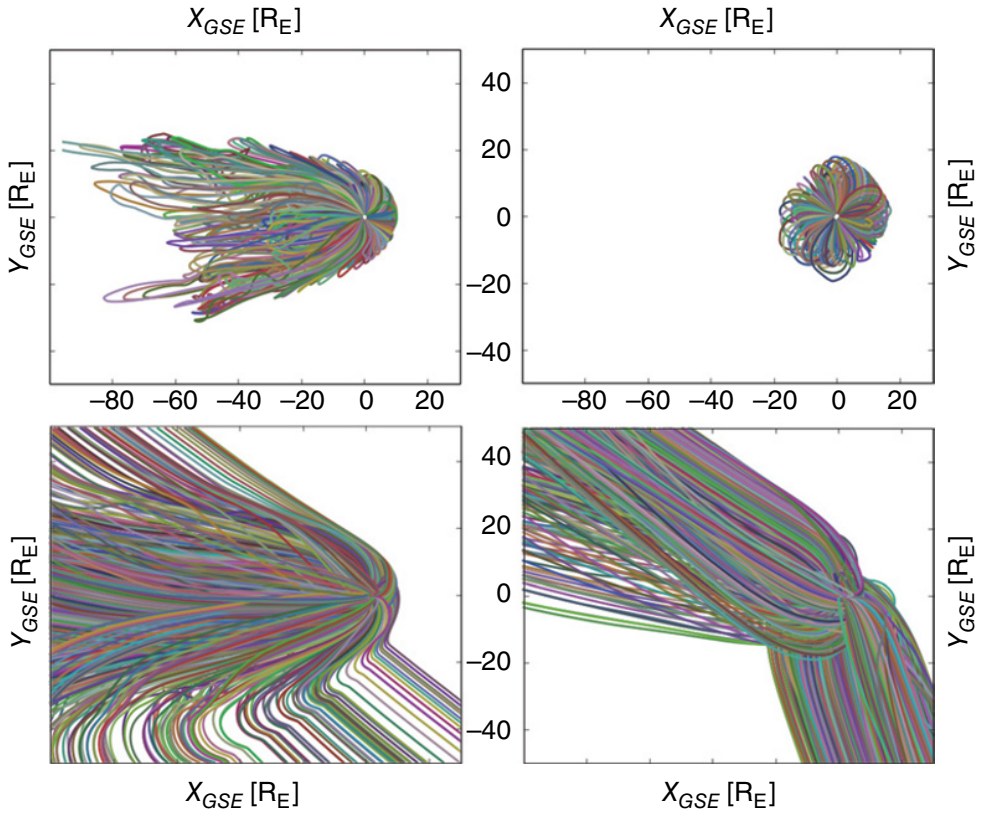

Figure 1.6 Top view of the magnetic field lines in the *Chané et al.* [2015] global MHD simulation. Top panels: closed magnetic field lines. Bottom panels: open magnetic field lines (only one side is connected to the ionosphere). Left panels: before the sub-Alfvénic flow reached the Earth's magnetosphere. Right panels: after the sub-Alfvénic flow reached the Earth's magnetosphere. The colors of the magnetic field lines have no specific meaning. The solar wind is coming from the right.

has its typical shape (see upper left panel of Fig. 1.6) because the solar wind ram pressure tends to compress the magnetosphere on the dayside and to stretch it on the nightside. On the other hand, when the solar wind Alfvén Mach number is lower than one, the solar wind magnetic pressure is more important than the solar wind ram pressure and therefore cannot be neglected any more. And since the solar wind magnetic pressure compresses the field lines, not only on the dayside, but also on the nightside, the closed field line region becomes very symmetric as shown in the upper right panel of Figure 1.6.

The open magnetic field lines are also affected by the transition from a super-Alfvénic to a sub-Alfvénic regime. While the open field lines first connect to the lobes and are then bent toward the equatorial plane to eventually connect to the interplanetary magnetic field in the super-Alfvénic case (bottom left panel of Fig. 1.6), they all point in the direction of the Alfvén wings for the sub-Alfvénic case (see bottom right panel of Fig. 1.6). The lobes actually disappear when the solar wind turns sub-Alfvénic, or to be more precise, the lobes are separated and form the two Alfvén wings. The same effect was shown by *Ridley* [2007] for simulations of the Earth's magnetosphere when the interplanetary magnetic field strength varies from 5 nT up to 100 nT, causing the solar wind to become sub-Alfvénic (see Fig. 7 from his article). In the *Ridley* [2007] case, dawn-dusk asymmetries are not present because the IMF in his simulations is perpendicular to the solar wind plasma flow, but our case is strongly asymmetric.

Chané et al. [2015] also investigated with their simulations how the field aligned currents change when the solar wind becomes sub-Alfvénic. They found that the currents were approximately 50% weaker in the sub-Alfvénic case, which is consistent with the disappearance of auroral activity during the May 2002 event reported by *Chané et al*. [2012]. In their simulation the transition from a super-Alfvénic solar wind to a sub-Alfvénic one was obtained by decreasing the solar wind density (similar to the conditions during the May 2002 event) while the interplanetary magnetic field was kept constant. If the sub-Alfvénic conditions had been caused by a strengthening of the interplanetary magnetic field, an enhancement of the field aligned currents would have been observed (as demonstrated by the simulations of *Ridley* [2007]).

Chané et al. [2015] also checked whether the sign of B_z in the solar wind had an important effect for the May 2002 event. They performed another simulation where they flipped B_z in the solar wind. They found almost no difference with the first simulation, although the nightside downward currents were approximately 30% weaker, indicating an higher (but still very weak) reconnection rate in the tail. Changing the sign of B_z in the solar wind resulted in only a 10° shift in the orientation of the interplanetary magnetic field (which was mostly in the direction of the Parker spiral), which explains why it had so little effect on the magnetosphere.

1.6. CONCLUSIONS

Long periods of sub-Alfvénic solar wind conditions at Earth are rare (once every 2.2 years in average) and are usually caused by a drastic drop in the solar wind density. During these events, the Earth loses its bow shock, the magnetosphere expands on the dayside and shrinks on the nightside, and two Alfvén wings are generated. Inside the Alfvén wings, the plasma speed drops and the magnetic field experiences a rotation. Usually, these sub-Alfvénic events introduce a strong dawn-dusk asymmetry in the magnetosphere, with the two wings pointing in widely different directions and having different properties (e.g., different plasma speeds). During the 24–25 May 2002 event, the solar wind Alfvén Mach number was as low as 0.4. It was estimated that the wings reached the size of 600 R_E (in the directions of the Alfvén characteristics $\mathbf{C}_A^{\pm}$ sketched in Fig. 1.1) and that the plasma speeds in the dawn and in the dusk Alfvén wings were 43% and 70% of the solar wind speed, respectively. During this event, the Geotail spacecraft crossed the Alfvén wings multiple times. IMAGE WIC images showed that there was almost no auroral activity during this event.

The May 2002 event has been studied in detail (mostly because of the abundance of in situ measurements available during these 2 days) but other events were more spectacular. For instance, during 4 July 1979, the Earth would theoretically have Alfvén wings 4000 R_E long under the assumption of steady-state homogeneous solar wind conditions (note that the Alfvén wings might have run into a denser plasma farther upstream while the interaction was still sub-Alfvénic at Earth). New sub-Alfvénic solar wind conditions at Earth are bound to happen again. Hopefully, in situ measurements at suitable position will be available to better understand Alfvén wings at Earth and the transition from a superfast to a sub-Alfvénic interaction.

It should also be noted that even if we understand that sub-Alfvénic periods in the solar wind are most of the time caused by a low density in the solar wind, why the solar-wind density becomes so low during these events remains an open question.

ACKNOWLEDGMENTS

Emmanuel Chané was funded by the Research Foundation-Flanders (grant FWO 441 12M0115N). Work at UNH was supported by grant AGS-11433895 from the National Science Foundation. Computations were performed on Trillian, a Cray XE6m-200 supercomputer at UNH supported by the NSF MRI program under grant PHY-1229408.

REFERENCES

Balasubramanian, V., P. Janardhan, S. Srinivasan, and S. Ananthakrishnan (2003), Interplanetary scintillation observations of the solar wind disappearance event of May 1999, *J. Geophys. Res. Space Physics*, *108*, 1121; doi:10.1029/2002JA009516.

Bonfond, B., D. Grodent, J. C. Gérard, A. Radioti, J. Saur, and S. Jacobsen (2008), UV Io footprint leading spot: A key feature for understanding the UV Io footprint multiplicity?, *Geophys. Res. Lett*., *35*, L05107; doi:10.1029/2007GL032418.

Bonfond, B., J. C. Gérard, D. Grodent, and J. Saur (2007), Ultraviolet Io footprint short timescale dynamics, *Geophys. Res. Lett*., *34*, L06201; doi:10.1029/2006GL028765.

Chané, E., J. Raeder, J. Saur, F. M. Neubauer, K. M. Maynard, and S. Poedts (2015), Simulations of the Earth's magnetosphere embedded in sub-Alfvénic solar wind on 24 and 25 May 2002, *J. Geophys. Res. Space Physics*, *120* (10), 8517–8528; doi:10.1002/2015JA021515. 2015JA021515.

Chané, E., J. Saur, F. M. Neubauer, J. Raeder, and S. Poedts (2012), Observational evidence of Alfvén wings at the Earth, *J. Geophys. Res. Space Physics*, *117*, A09217; doi:10.1029/2012JA017628.

Clarke, J. T., J. Ajello, G. Ballester, L. Ben Jaffel, J. Connerney, J. C. Gérard, G. R. Gladstone, D. Grodent, W. Pryor, J. Trauger, and J. H. Waite (2002), Ultraviolet emissions from the magnetic footprints of Io, Ganymede and Europa on Jupiter, *Nature*, *415*, 997–1000.

Drell, S. D., H. M. Foley, and M. A. Ruderman (1965), Drag and propulsion of large satellites in the ionosphere: An Alfvén propulsion engine in space, *J. Geophys. Res*., *70*, 3131–3145; doi:10.1029/JZ070i013p03131.

Duling, S., J. Saur, and, J. Wicht (2014), Consistent boundary conditions at nonconducting surfaces of planetary bodies: Applications in a new Ganymede MHD model, *J. Geophys. Res. Space Physics*, *119*, 4412–4440; doi:10.1002/2013JA019554.

Frank, L. A., and W. R. Paterson (2000), Return to Io by the *Galileo* spacecraft: Plasma observations, *J. Geophys. Res*., *105*, 25 363–25 378; doi:10.1029/1999JA000460.

Gérard, J. C., A. Saglam, D. Grodent, and, J. T. Clarke (2006), Morphology of the ultraviolet Io footprint emission and its control by Io's location, *J. Geophys. Res. Space Physics*, *111*, A04202; doi:10.1029/2005JA011327.

Gérard, J. C., J. Gustin, D. Grodent, P. Delamere, and, J. T. Clarke (2002), Excitation of the FUV Io tail on Jupiter: Characterization of the electron precipitation, *J. Geophys. Res. Space Physics*, *107*, 1394; doi:10.1029/2002JA009410.

Gosling, J. T., J. R. Asbridge, S. J. Bame, W. C. Feldman, R. D. Zwickl, G. Paschmann, N. Sckopke, and C. T. Russell (1982), A sub-Alfvénic solar wind: Interplanetary and magnetosheath observations, *J. Geophys. Res*., *87*, 239–245; doi:10.1029/JA087iA01p00239.

Jia, X., R. J. Walker, M. G. Kivelson, K. K. Khurana, and J. A. Linker (2009), Properties of Ganymede's magnetosphere inferred from improved three-dimensional MHD simulations, *J. Geophys. Res. Space Physics*, *114*, A09209; doi:10.1029/2009JA014375.

Jordanova, V. K., C. J. Farrugia, J. F. Fennell, and J. D. Scudder (2001), Ground disturbances of the ring, magnetopause, and tail currents on the day the solar wind almost disappeared, *J. Geophys. Res*., *106*, 25 529–25 540; doi:10.1029/2000JA000251.

Kivelson, M. G., F. Bagenal, W. S. Kurth, F. M. Neubauer, C. Paranicas, and J. Saur (2004), Magnetospheric interactions with satellites, in *Jupiter, The Planet, Satellites and Magnetosphere*, edited by F. Bagenal, T. E. Dowling, and W. B. McKinnon, 513–536.

Kopp, A., S. Schilp, and S. Preusse (2011), Magnetohydrodynamic simulations of the magnetic interaction of hot Jupiters with their host stars: A numerical experiment, *Astrophys. J*., *729*, 116; doi:10.1088/0004- 637X/729/2/116.

Lavraud, B., and J. E. Borovsky (2008), Altered solar wind-magnetosphere interaction at low Mach numbers: Coronal mass ejections, *J. Geophys. Res. Space Physics*, *113*, A00B08; doi:10.1029/2008JA013192.

Lavraud, B., E. Larroque, E. Budnik, V. Génot, J. E. Borovsky, M. W. Dunlop, C. Foullon, H. Hasegawa, C. Jacquey, K. Nykyri, A. Ruffenach, M. G. G. T. Taylor, I. Dandouras, and H. Rème (2013), Asymmetry of magnetosheath flows and magnetopause shape during low Alfvén Mach number solar wind, *J. Geophys. Res. Space Physics*, *118*, 1089–1100; doi:10.1002/jgra.50145.

Lavraud, B., J. E. Borovsky, A. J. Ridley, E.W. Pogue, M. F. Thomsen, H. Rème, A. N. Fazakerley, and E. A Lucek (2007), Strong bulk plasma acceleration in Earth's magnetosheath: A magnetic slingshot effect?, *Geophys. Res. Lett*., *34*, L14102; doi:10.1029/2007GL030024.

Le, G., C. T. Russell, and S. M. Petrinec (2000b), The magnetosphere on May 11, 1999, the day the solar wind almost disappeared: I. Current systems, *Geophys. Res. Lett*., *27*, 1827–1830; doi:10.1029/1999GL010774.

Le, G., P. J. Chi, W. Goedecke, C. T. Russell, A. Szabo, S. M. Petrinec, V. Angelopoulos, G. D. Reeves, and F. K. Chun (2000a), Magnetosphere on May 11, 1999, the day the solar wind almost disappeared: II. Magnetic pulsations in space and on the ground, *Geophys. Res. Lett*., *27*, 2165–2168; doi:10.1029/1999GL000012.

Linker, J. A., M. G. Kivelson, and R. J. Walker (1988), An MHD simulation of plasma flow past Io-Alfvén and slow mode perturbations, *Geophys. Res. Lett*., *15*, 1311–1314; doi:10.1029/GL015i011p01311.

Neubauer, F. M. (1980), Nonlinear standing Alfven wave current system at Io: Theory, *J. Geophys. Res*., *85*, 1171–1178; doi:10.1029/JA085iA03p01171.

Neubauer, F. M. (1998), The sub-Alfvénic interaction of the Galilean satellites with the Jovian magnetosphere, *J. Geophys. Res*., *1031*, 19 843–19 866; doi:10.1029/97JE03370.

Nishino, M. N., M. Fujimoto, T. D. Phan, T. Mukai, Y. Saito, M. M. Kuznetsova, and L. Rastätter (2008), Anomalous flow deflection at Earth's low-Alfvén-Mach-number bow shock, *Phys. Rev. Lett*., *101* (6), 065003; doi:10.1103/PhysRevLett.101.065003.

Ohtani, S., P. T. Newell, and K. Takahashi (2000), Dawn-dusk profile of field-aligned currents on May 11, 1999: A familiar pattern driven by an unusual cause, *Geophys. Res. Lett*., *27*, 3777–3780; doi:10.1029/2000GL003789.